

MICROBIOLOGY

N-terminal signal peptides facilitate the engineering of PVC complex as a potent protein delivery system

Feng Jiang^{1*†}, Jiawei Shen^{1†}, Jiaxuan Cheng^{2,3†‡}, Xia Wang¹, Jianguo Yang⁴, Ningning Li², Ning Gao², Qi Jin^{1*}

Extracellular contractile injection systems (eCISs) are widespread bacterial nanomachines that resemble T4 phage tail. As a typical eCIS, *Photorhabdus* virulence cassette (PVC) was proposed to inject toxins into eukaryotic cells by puncturing the cell membrane from outside. This makes it an ideal tool for protein delivery in biomedical research. However, how to manipulate this nanocomplex as a molecular syringe is still undetermined. Here, we identify that one group of N-terminal signal peptide (SP) sequences are crucial for the effector loading into the inner tube of PVC complex. By application of genetic operation, cryo-electron microscopy, in vitro translocation assays, and animal experiments, we show that, under the guidance of the SP, numerous prokaryotic and eukaryotic proteins can be loaded into PVC to exert their functions across cell membranes. We therefore might customize PVC as a potent protein delivery nanosyringe for biotherapy by selecting cargo proteins in a broad spectrum, regardless of their species, sizes, and charges.

INTRODUCTION

Bacteria produce multiple nanodevices to deliver protein substrates, including toxins, signal molecules, and antibodies into the cytoplasm by creating a pore across the plasma membrane. These devices could be manipulated to overcome the low efficiency of penetrating the cell membrane during translocating proteins, but they have drawbacks. Individual evidence has been shown to apply type VI secretion system (T6SS) for antigen/toxin delivery into target cells (1, 2). Another highly coordinated nanomachine, T3SS, has likewise been used as a promising tool for direct protein delivery into the cytosol of host cells (3, 4). Heterologous proteins labeling with a secretion tag or fusing to a native effector were capable of secretion through the T3SS injectisome (5, 6). However, the application of cytotoxic bacterial strain for delivery and low efficiencies of production and translocation of certain foreign proteins still hinder the wide utilization of T3SS. In addition, tripartite toxin complexes (Tcs), originally found in the genus *Photorhabdus* (7–9), were engineered recently to transport proteins across the membrane other than its natural effectors (10, 11). Similarly, rigorous criteria (protein size, net charge, and structural conformation of the cargo) must be fulfilled to set up a functional Tc injection device (10).

Previously, the overall structure of *Photorhabdus* virulence cassette (PVC) [a typical extracellular contractile injection system (eCIS)] in the extended and contracted state has been resolved (12), and PVC was identified as the causative agent of *Photorhabdus* pathogenicity (13, 14). Because the PVC has a simplified phage tail-like architecture with capacious inner lumen and can be released outside bacterial cells for puncturing reaction (15), it would be an ideal model for manipulation as an in vitro protein delivery system. Here, we

identified an essential N-terminal signal peptide (SP) encoded within the PVC effector sequence, which plays a critical role in stabilizing and loading of the substrate into the nanodevice. By fusing the SP to the N terminus of heterologous proteins, they can be recognized by the PVC complex and secreted via the nanosyringe. Unexpectedly, unlike other systems, which have strict guidelines for selecting substrates, the PVC complexes can load a broad range of SP-tagged proteins regardless of their species, sizes, net charges, and conformations. The loading of cargoes was specifically dependent on the presence of N-terminal SP, and the existence of the ATPases associated with a variety of cellular activities (AAA) domain-containing protein encoded in the PVC locus (Pvc15). Other adenosine triphosphatases (ATPases) from different secretion systems seemingly could not fulfill this assignment. The loading status was further illustrated by cryo-electron microscopy (cryo-EM) analysis. Last, the system was manipulated to translocate a eukaryotic toxin for tumor therapy in a mouse model, demonstrating the potent applications of this nanosyringe in drug delivery and biomedication.

RESULTS

Identification of the N-terminal SP in PVC effectors

Five Pvc clusters (PVC-I to PVC-V) are encoded within the *Photorhabdus asymbiotica* chromosome (16), and several putative effector genes can be found downstream the respective locus (fig. S1A). Two effectors, *photorhabdus* necrotizing factor (Pnf) and *photorhabdus* dNTP pyrophosphatase 1 (Pdp1), can be loaded and translocated by PVC-V complex (hereafter PVC unless indicated) for cytotoxicity (13). Through comparison between the PVC effectors and their homologs, we have found that a typical extra N-terminal fragment can be defined within the protein sequences of PVC effectors (Fig. 1A). We hypothesized that these N-terminal sequences are necessary for effector loading.

To investigate the detailed mechanism of effector loading, we immunoprecipitated C-terminal Flag-tagged Pnf and Pdp1 proteins in the bacterial strains producing loaded PVC particles. A clear smaller protein band can be observed from both immunoprecipitations, indicating that a possible cleavage event occurs during effector loading

Copyright © 2022
The Authors, some
rights reserved;
exclusive licensee
American Association
for the Advancement
of Science. No claim to
original U.S. Government
Works. Distributed
under a Creative
Commons Attribution
NonCommercial
License 4.0 (CC BY-NC).

¹NHC Key Laboratory of Systems Biology of Pathogens, Institute of Pathogen Biology, Chinese Academy of Medical Sciences & Peking Union Medical College, Beijing, P. R. China. ²State Key Laboratory of Membrane Biology, Peking-Tsinghua Center for Life Sciences, School of Life Sciences, Peking University, Beijing, P. R. China. ³Tsinghua-Peking Center for Life Sciences, School of Life Sciences, Tsinghua University, Beijing, P. R. China. ⁴State Key Laboratory of Protein and Plant Gene Research, School of Advanced Agricultural Sciences, Peking University, Beijing, P. R. China.

*Corresponding author. Email: jiangfenguva@126.com (F.J.); zdsys@vip.sina.com (Q.J.)
†These authors contributed equally to this work.

‡Present address: Vaccine Research Center, National Institute of Allergy and Infectious Diseases, National Institutes of Health, Bethesda, MD 20892, USA.

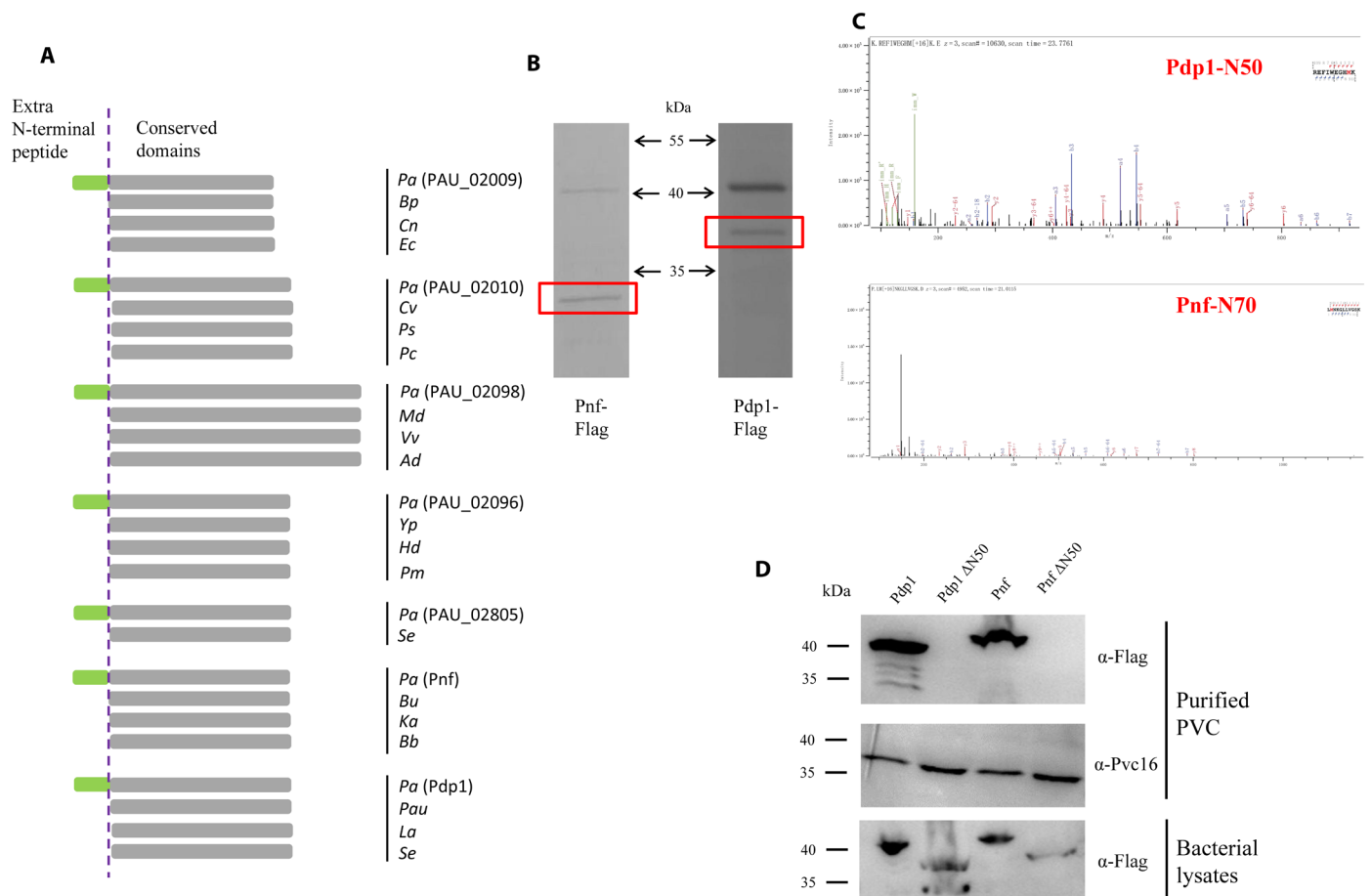


Fig. 1. Identification of the N-terminal SP within PVC effectors. (A) Schematic illustration of the extra N-terminal peptides in the PVC effectors when comparing with their homologs. *Pa*, *Photobacterium aerophilum*; *Bp*, *Burkholderia pseudomallei*; *Cn*, *Cedecea neteri*; *Ec*, *Escherichia coli*; *Cv*, *Chromobacterium vaccinii*; *Ps*, *Providencia stuartii*; *Pc*, *Pseudomonas cichorii*; *Md*, *Moritella dasanensis*; *Vv*, *Vibrio vulnificus*; *Ad*, *Aeromonas dhakensis*; *Yp*, *Yersinia pestis*; *Hd*, *Haemophilus ducreyi*; *Pm*, *Pasteurella multocida*; *Se*, *Salmonella enterica*; *Bu*, *Burkholderia ubonensis*; *Ka*, *Klebsiella aerogenes*; *Bb*, *Bordetella bronchiseptica*; *Pau*, *Photobacterium australe*; *La*, *Lysobacter antibioticus*. (B) Immunoprecipitation of the loaded Pdp1 and Pnf proteins with Flag magnetic beads. The predicted sizes of full-length Pnf and Pdp1 are 36.7 and 37.2 kDa, respectively, as shown in table S1. The minor cleaved protein bands can be observed clearly (red box). (C) Mass spectrometry analysis for the N-terminal sequence of the cleaved bands from Pdp1 or Pnf immunoprecipitates in (B). (D) The effectors with or without 50 N-terminal amino acids were probed in bacterial lysates and purified PVC. One of the PVC key components Pvc16 was used as a loading control. Representative pictures of at least three independent experiments are shown.

(Fig. 1B). To verify this, we cut out the small band and applied it for mass spectrometry (MS) analysis. The results showed that 50 or 70 N-terminal amino acids of Pdp1 or Pnf have been deleted (Fig. 1C), suggesting the potential involvement of its N-terminal sequence for effector loading. We then asked whether the N terminus acts as a SP for PVC loading. Although the protein stability of Pdp1 was affected slightly by the N-terminal deletion (Pdp1 Δ N50; fig. S1B), the truncated Pdp1 effector cannot be loaded into PVC complex completely (Fig. 1D). As for Pnf, deletion of N70 totally abrogates the production of detectable protein (fig. S1C). Alternatively, Pnf Δ N50 displayed similar characteristics as the Pdp1 Δ N50 (fig. S1, B and C), and this mutant cannot be loaded into PVC as well (Fig. 1D). Hence, we speculated that the 50 N-terminal amino acids of Pnf and Pdp1 possibly act as the SP for cargo loading into PVC particles.

N50-SP fused reporter proteins can be loaded and translocated by PVC complex

Because PVC complex shared great similarity with T4 phage tail and could be produced abundantly in vitro, we wondered whether

it can be manipulated as a molecular syringe for protein injection under the guidance of the N-terminal SP. We then created several N-terminal SP fused proteins with BlaM (β -lactamase), monomeric red fluorescent protein (mRFP), Nanoluc (Nanoluciferase), or Rluc (*Renilla* luciferase), all of which are widely used as sensitive reporters in biological research (Fig. 2A). At the beginning, all the fusion proteins were successfully loaded into the PVC complex under the guidance of Pnf or Pdp1 N50-SP (Fig. 2B). Pnf and Pdp1 effectors were previously proven to be injected by the PVC complex into J774 murine macrophages (13). To test the effects of reporters after PVC delivery, we treated J774 with relative PVC solutions, and relevant measurements were carried out. The results showed that SP-fused Rluc (Fig. 2C) and BlaM (Fig. 2, D and E), but not those without N-terminal SP, can be translocated into eukaryotic cells in a dose-dependent manner, suggesting their effectiveness in these applications. Further, to ask whether any key residues play crucial role in cargo loading, we performed multiple sequence alignments with the N50-SPs from putative PVC effectors in the sequenced *Photobacterium* genomes, and alanine scanning with Pnf N50-SP was also conducted.

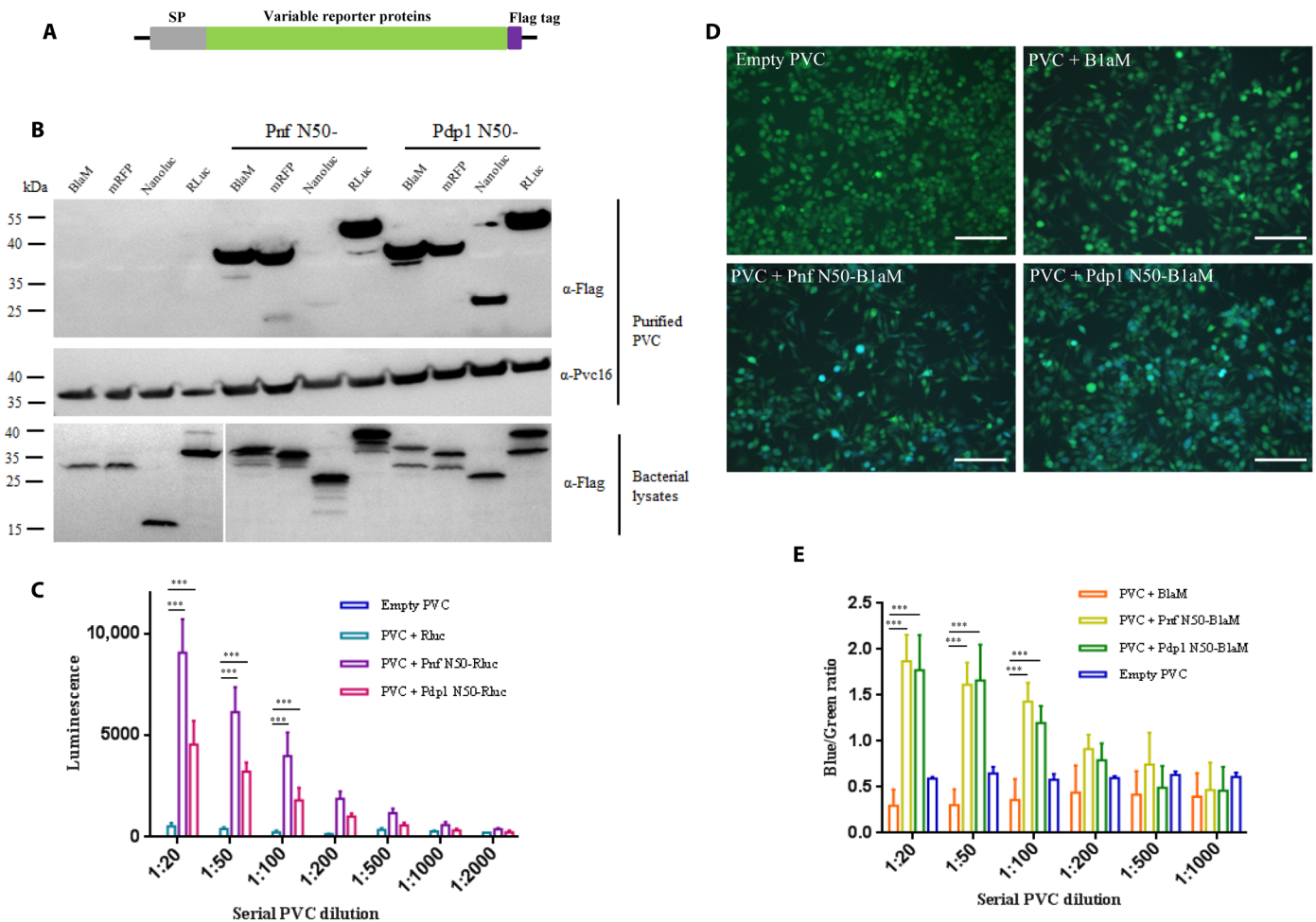


Fig. 2. Loading and translocation of reporter proteins by PVC. (A) Diagram of the N-terminal SP-fused construct for various reporter proteins. A Flag tag was added at the C terminus. (B) Loading status of reporter proteins (BlaM, mRFP, Nanoluc, and RLuc) under the guidance of Pnf or Pdp1 N50-SP into PVC complex was detected by Western blot. Pvc16 was used as a loading control. (C) Monitor of the luminescence in the J774 host cells treated by serial concentration of PVC solutions containing RLuc. The initial concentration of PVC solution was 5 mg ml^{-1} . Error bars show the means and SD of three independent experiments ($n = 3$). Statistical analysis was performed between samples with (Pnf N50 or Pdp1 N50) and without SP sequence. (D) Fluorescent microscopic graphs of J774 treated with PVC containing BlaM cargoes. Scale bar, $50 \mu\text{m}$. (E) The ratio of blue (450 nm) to green (520 nm) fluorescence in J774 was determined after treatment of serial PVC dilution, indicating the SP-guided BlaM translocation by PVC into host cells. Error bars show the means and SD of three independent experiments ($n = 3$). Statistical analysis was performed between samples with (Pnf N50 or Pdp1 N50) and without SP sequence.

Rare conserved residues can be defined in the SP sequences, and the loading efficiency was not affected by any point mutations within the N50-SP (fig. S2, A and B). The overall PVC structures were not changed after SP-guided protein loading as well (fig. S2C). Thus, our data suggested that the N-terminal SP can be used as a guide for cargo loading into PVC syringe, and this loading recognition was not determined by any single residue within the coding sequence.

N50-SP guided PVC loading and delivery of bacterial effectors

To achieve the goal of engineering PVC as an efficient delivery system for diverse purposes, we further explore the SP-guided loading of multiple effectors from several bacterial secretion systems (T3SS, T4SS, T6SS, and T7SS), whose functions have been validated extensively and are applied in distinct biomedical treatments. For T3SS effectors, we selected proteins from several important pathogens varying from 27.8 to 130 kDa in predicted molecular weights (MWs) and 4.63 to 9.10 in predicted isoelectric points (PI) (table S1). The results

demonstrated that they can all be loaded into the PVC complex under the guidance of N-terminal Pnf or Pdp1 N50-SP (Fig. 3A). Exoenzyme U (ExoU) from *Pseudomonas aeruginosa* T3SS has phospholipase A_2 activity that cause instant lysis of host cells (17, 18), and substantial cell death was observed when cells were treated by PVC with ExoU in the cytotoxicity assays (Fig. 3B and fig. S3A). Non-LEE-encoded effector C (NleC) from *Escherichia coli* T3SS is a metalloprotease that specifically cleaves p65 in host cells to modulate nuclear factor κB signaling pathway (19), and p65 protein was indeed degraded by PVC with NleC toxin (Fig. 3C). The overall PVC structures were also not affected by the effector loadings, irrespective of the cargo sizes (fig. S3B). In the case of T4SS (Fig. 3, D and E), T6SS (Fig. 3F) and T7SS (Fig. 3, G and H) effectors, similar outcomes were obtained when MWs and PIs are ranging from 9.9 to 132.3 kDa and 4.48 to 9.88, respectively (table S1). Cytotoxin-associated gene A (CagA) is a major virulence factor of *Helicobacter pylori* T4SS that can interact with the hepatocyte

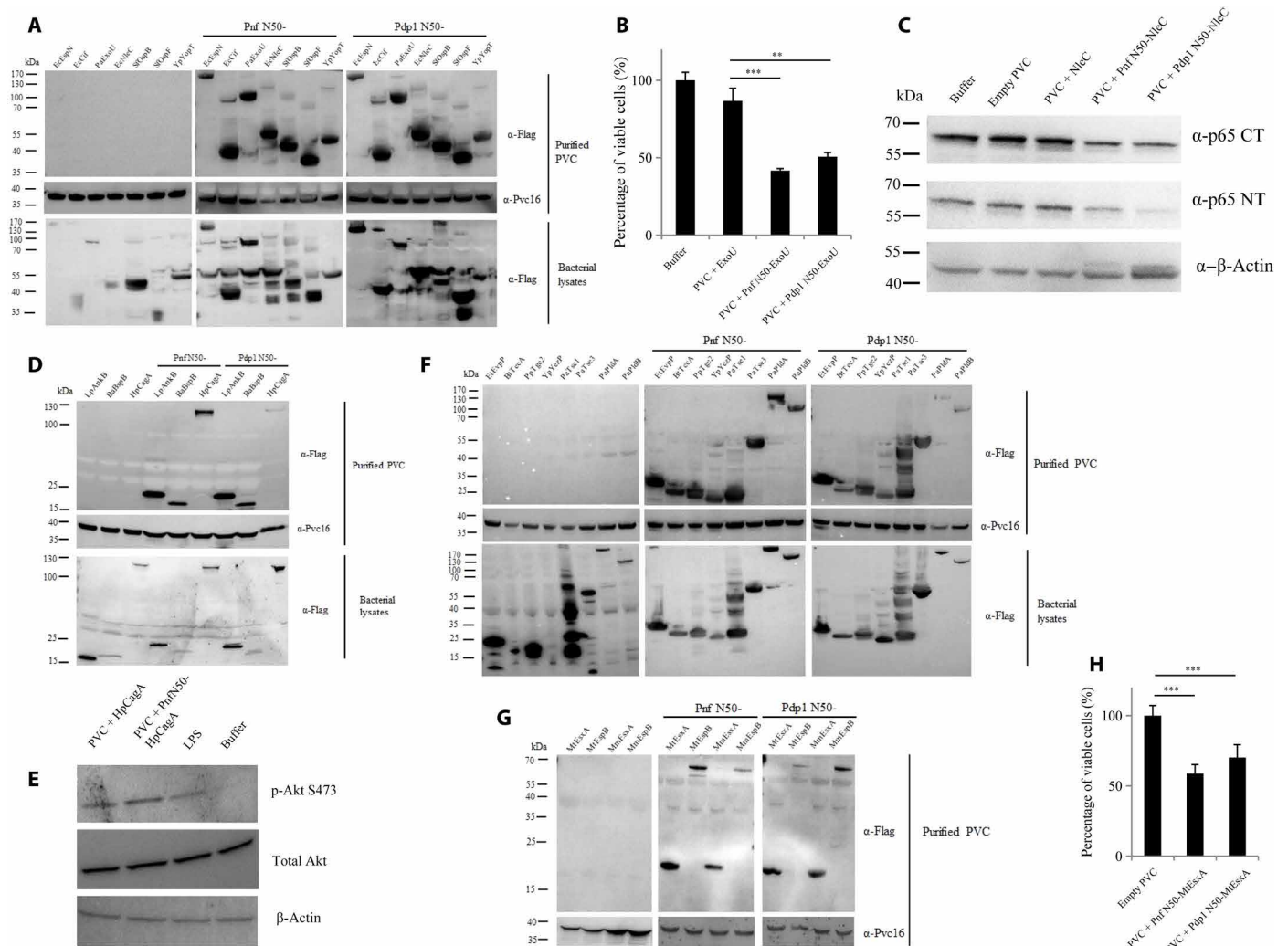


Fig. 3. Loading and translocation of effectors from T3SS, T4SS, T6SS, and T7SS. (A) Loading of diverse T3SS effectors into PVC under the guidance of Pnf or Pdp1 N50-SP. (B) Cytotoxicity assays of J774 host cells after treatment with PVC harboring ExoU for 24 hours. Cell viability was measured using water-soluble tetrazolium 8 (WST-8) as the substrate. The concentration of PVC solution for each sample was $250 \mu\text{g ml}^{-1}$. Error bars show the means and SD of three independent experiments ($n = 3$). (C) p65 proteins from nuclear factor κB signaling pathway in host cells were cleaved by PVC-delivered NleC effectors. (D) Loading of several T4SS effectors into PVC complex by SP guidance. (E) Akt proteins from host cells were activated by PVC-delivered *Helicobacter pylori* CagA effectors. J774 cells were treated with relative PVC solutions for 30 min, and lipopolysaccharide (LPS) ($50 \mu\text{g ml}^{-1}$) was used as positive control. (F) Loading of multiple T6SS effectors into PVC complex. (G) Loading of T7SS effectors from *Mycobacteria* into PVC complex by SP guidance. (H) Cytotoxicity assays after treatment with PVC harboring ExsA from *Myc*

draw the conclusion that PldA is indeed inside of the lumen. The cargo density is highlighted and displayed at a different contour level in longitudinal central sections of the PVC-PldA density maps (Fig. 4, B, C, E, and F). Although the PldA MW is three times larger than that of Pnf and Pdp1, its densities could also be detected in the baseplate and sheath-tube trunk in a nonuniform pattern, which is similar to the status of small effectors reported before (13). This outcome further validated the previous models that PVC cargoes are likely loaded in unfolded forms in the lumen. In addition, taking into account that the loaded proteins were fitted in a nonuniform pattern, we speculated that there might be certain factors that play a role in unfolding the cargoes (probably from the cap site) and inserting them into the PVC lumen.

Pvc15 is essential for SP recognition and cargo loading

ATPase proteins are important in providing energy for bacterial secretion systems, albeit with different modes of action (25–27). In

the context of PVC structure proteins, Pvc15 (PAU_03339) is predicted to be an AAA+ ATPase family protein (Fig. 5A), which could be the energy source of PVC loading. Bioinformatic analysis showed that Pvc15 is more closely related to the FtsH_3 or HflB_2, which acts as a processive metalloprotease for degrading integral membrane proteins (Fig. 5B). We then deleted Pvc15 in the complete PVC locus, which expresses both structural and effector genes. Western blot detection showed that Pvc15 is critical for cargo loading. Complementation of Pvc15, but not other ATPases from T3SS, T4SS, or T6SS, could restore the cargo loading in PVC (Fig. 5C). To further explore the function of Pvc15, we constructed plasmids coproducing Pvc15 and mRFP with variable N-terminal SP to decide the influence of Pvc15 toward protein folding (Fig. 5D). The mRFP fluorescence was then monitored in the bacterial strains harboring different inducible plasmids, respectively. The results showed that the relative red fluorescence intensity decreased markedly from the

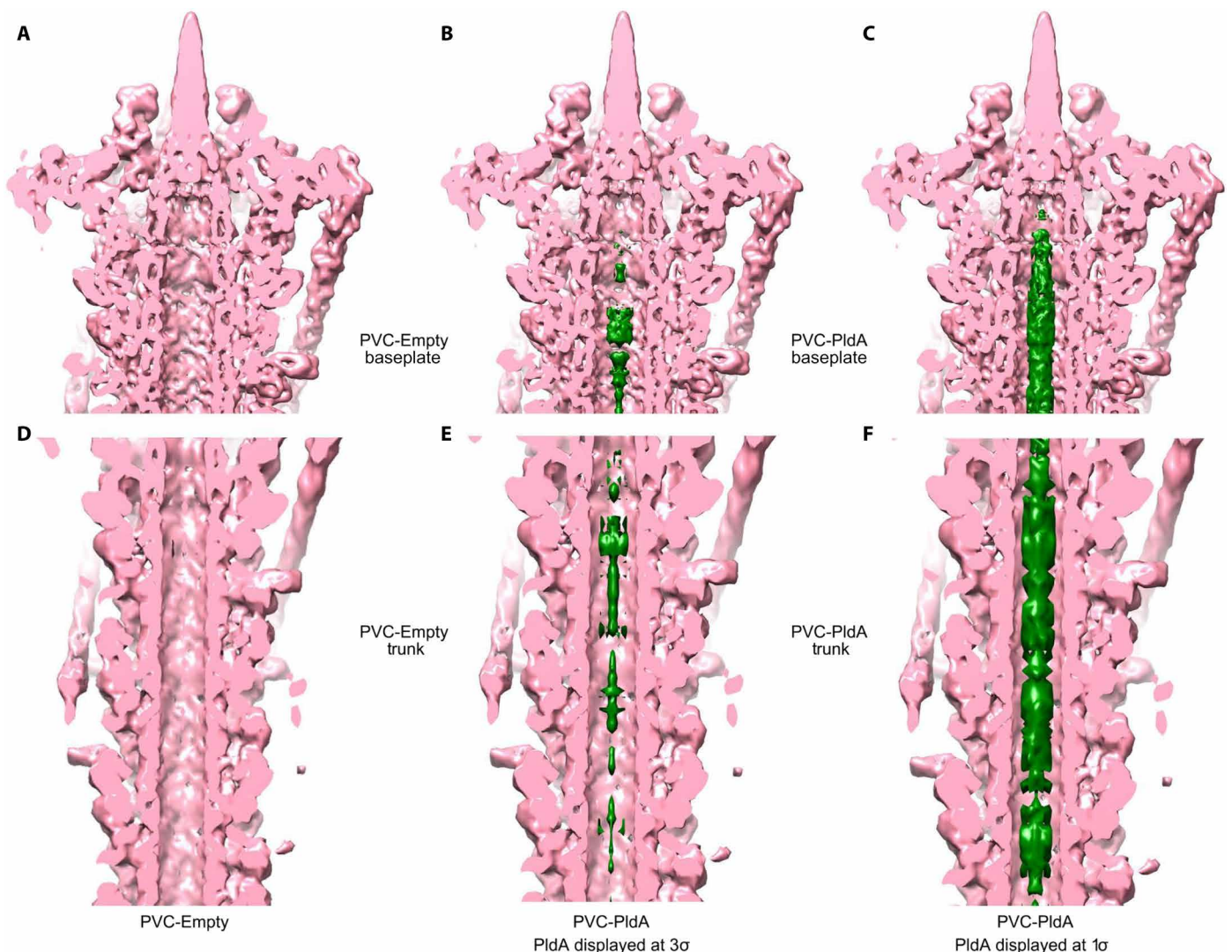


Fig. 4. Cryo-EM analysis of Pnf N50-SP-guided loading of PldA in PVC. (A to F) Longitudinal central sections of the PVC density maps for the PldA samples in the baseplate (A to C) and sheath-tube trunk (D to F) regions. For clarity of cargo display, the density maps of the empty PVC baseplate and trunk (EMD-31358 and EMD-31359) are filtered to the same resolution as the ones from the PldA sample. For the PVC-PldA sample, cargo density is highlighted in forest displayed at a contour level of 3σ (B and E) or 1σ (C and F) level.

construct fused with Pdp1 or Pnf N50-SP after a period of incubation, when compared with the construct without N-terminal signal or Pvc15 protein (Fig. 5E). In addition, the reduction of mRFP signal was not due to the differential protein productions in these cultures (fig. S5). Although conserved Walker A and Walker B motifs of ATPase can be predicted within the Pvc15 sequence (Fig. 5A), we failed to abolish the activity of Pvc15 by point mutations. We speculate that there may be some other mechanisms affecting the activity of this protein. Alternatively, we have included the constructs without Pvc15 for negative controls (Fig. 5E). All these results suggested that Pvc15 is possibly involved in recognizing the SP and unfolding the protein for subsequent PVC loading (Fig. 5F).

Eukaryotic proteins loading into PVC and antitumor application in mouse model

To explore the variety of loading substrates in PVC complex, we tested several eukaryotic proteins from mammal, plant, protozoan, and fungus. All these proteins in a wide range of MWs and PIs can

also be loaded and translocated by PVC under the guidance of N-terminal SP (Fig. 6A and fig. S6, A and B). This encouraged us to examine its application of antitumor drug loading and delivery in animal model. We tested several toxic proteins and found that trichosanthin from *Trichosanthes kirilowii* (TcsT), which is a type I ribosome-inactivating protein, display the best killing effect toward J774 cells in the in vitro assays. TcsT has also been used previously for anticancer therapy (28, 29). In addition, J774 is a mouse-originated tumor cell, so we can easily apply it into the animal models for PVC function validation. Pnf N50-SP-fused TcsT was successfully fit in the PVC particles (Fig. 6B), and the number of viable J774A.1 cells decreased remarkably after PVC + TcsT treatment using the Cell Counting Kit-8 (Fig. 6C). The antitumor effect was then evaluated in the BALB/c mice bearing J774A.1 tumors (five mice per group; Fig. 6D). The results demonstrated that intratumoral PVC + TcsT injections after 2 weeks yield significant antitumor activity in the mice, and the tumor growth could not be inhibited by administration of PVC solution alone (Fig. 6 and fig. S7). This suggests that

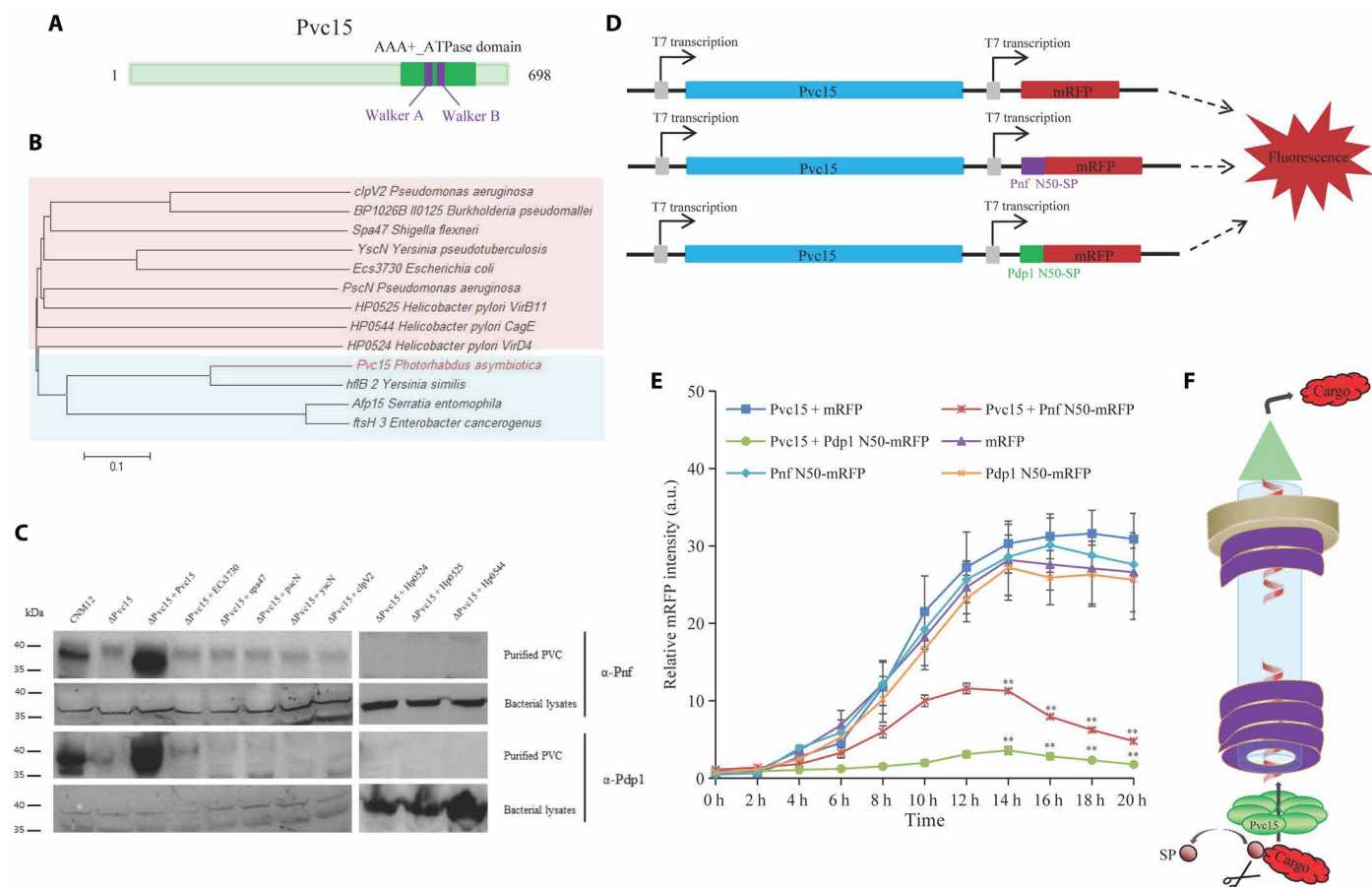


Fig. 5. ATPase Pvc15 is essential for cargo loading. (A) Schematic diagram of Pvc15 protein. Pvc15 has one annotated AAA+ ATPase domain containing Walker A and Walker B motifs (ATPase family associated with various cellular activities, PF00004). (B) Phylogenetic analysis of Pvc15 with several important ATPases in other bacteria. The ATPases from T3SS, T4SS, and T6SS are included in the shaded red section. Pvc15 and its homologs are included in the shaded blue section. Pvc15 is highlighted in red. (C) Pvc15 was involved in PVC effector loading (Pnf and Pdp1), and this role cannot be replaced by ATPases from other secretion systems. (D) Illustration of the pETDuet-1 constructs coproducing Pvc15 and different mRFPs. (E) Pvc15 was capable of decreasing the fluorescence intensity of SP-fused mRFP variants. *E. coli* strain JM109 (DE3) harboring the respective plasmid construct in (D) was induced by 0.2 mM isopropyl- β -D-thiogalactopyranoside for 20 hours, and the mRFP fluorescence was monitored at 2-hour intervals. Plasmids expressing mRFP variants alone were used as no-Pvc15 controls. Error bars show the means and SD of three independent experiments ($n = 3$). Statistical analysis was performed between samples with and without SP sequence. a.u., arbitrary units. (F) Graphic model of how cargo is recognized and unfolded by Pvc15 to fit into the PVC complex and then delivered.

and prepared in the form of solutions, ignoring the complicated steps of purification. It is possible to customize the nanosyringe with different drugs in a large scale to meet the potential needs of industries. Third, PVC, as a potent delivery vector, showed low cytotoxicity to the target cells and hosts (Figs. 3B and 6E). The bacterial residual cytotoxicity always prevented us from carrying out a long period of time of incubation when using live strains with *in vivo* applications (T3SS, for instance) (3, 5, 37). Although more data will be needed for an affirmative answer, empty PVC in this study seems to overcome this disadvantage and is suitable for better utilizations.

Until recently, diverse sophisticated routes have been identified in the bacterial secretion systems to facilitate the effector delivery (38). In T3SS, noncleavable N-terminal sequences can be defined from their secretory proteins but share little conservative features from each other. Certain specialized accessory proteins called chaperones can associate with their cognate effectors. These specialized proteins are irreplaceable and indispensable for efficient substrate secretion (39). Several similar so-called chaperones are also found in T4SS, although their functions are not well established (40–42). In the field of T6SS, which have great structure similarities with PVC and other eCIS complexes (43), several types of mechanisms have been determined in assisting the effector secretion. Tec (DUF4123) family proteins displayed essential roles for T6SS-dependent loading of the effectors (44); Eag (DUF1795) family proteins engaged in stabilizing effectors and promoting T6SS delivery through the spike (45, 46); and a DUF2169 or DUF2875 protein has also been described as a chaperone or adaptor for T6SS substrates delivery (47, 48). However, the secretion machineries across all the systems discussed seemed to be somewhat complicated for future biological manipulation. PVC complex, and possibly other widespread eCIS nanoweapons, are just cell-free toxin delivery systems that are more easily to design and modify. Particularly, the customizable cargoes can be loaded into the PVC particle simply by adding an N-terminal SP to accomplish specific tasks, making this platform a handy and convenient tool under a wide range of conditions.

To sum up, with the help of N-terminal SP, we would be able to engineer PVC as a powerful device for protein or polypeptide injection into mammalian cells and eventually therapeutic utilizations. Concerning the flexibility of selecting variable cargoes and simplicity of production, we expect to manipulate this protein delivery toolkit into a versatile and easy-to-use nanosyringe for biomedical applications.

MATERIALS AND METHODS

Bacterial strains and cell lines

E. coli strains were cultured in LB broth at 37°C. *E. coli* strain Top10 was used for DNA manipulation, and *E. coli* EPI300 was used for PVC purification. Antibiotics were used as follows: ampicillin, 100 µg ml⁻¹; tetracycline, 10 µg ml⁻¹; kanamycin, 25 µg ml⁻¹; gentamycin, 20 µg ml⁻¹; chloramphenicol, 25 µg ml⁻¹. J774A.1 murine macrophage cell lines were cultured in Dulbecco's modified Eagle's medium (Thermo Fisher Scientific) supplemented with 10% fetal bovine serum (Gibco) and streptomycin-penicillin (Invitrogen).

Plasmid construction and DNA manipulation

pBBRN was generated by introducing a new Nde I site into the start codon of LacZα gene, to eliminate the previous N-terminal fusion of 20 amino acids. A FLAG tag sequence was also introduced to the

C-terminal end. DNA amplification was conducted using Q5 high-fidelity DNA polymerase (New England Biolabs), and the templates used were from genomic DNA or synthesized plasmid DNA, respectively (table S3). Amplified gene fragments were cloned into pBBRN with or without N-terminal SP of Pnf or Pdp1. Site-directed mutagenesis were conducted using the *Fast* Mutagenesis System (TransGen).

For the construction of pCNM3 and pBR60 expressing LysR regulator gene, detailed procedures can be referred previously (12, 13). To generate pCNM12 plasmid producing both PVC particle and its effectors, the genomic DNA fragment (PAU_03353 to PAU_03332) was cleaved using Cas9-Assisted Targeting of Chromosome Segments as described (49) and was ligated into the pRK404 for expression. The positive clones were confirmed by polymerase chain reaction (PCR) and enzyme digestion. For the creation of ΔPvc15 mutant in pCNM12, a Tn5 transposon insertion kit (Lucigen) was used following the supplier's protocols. The transposon insertion clones inactivating *pvc15* gene were selected by colony-PCR verifications.

PVC purification

The purification steps of PVC can be found in previous literature with minor modifications (12). Briefly, the LysR-producing plasmid pBR60 was transformed into *E. coli* EPI300 strain harboring plasmid pCNM3, which expresses PVC structural genes. If cargo protein was included, a third pBBRN plasmid expressing relevant genes was transformed into the strain as well. Overnight cultures were inoculated into 200 ml of LB broth for another 16-hour growth at 30°C. Bacterial pellets were collected and lysed in 30 ml of buffer P [25 mM tris (pH 7.4), 140 mM NaCl, 3 mM KCl, deoxyribonuclease I (50 µg ml⁻¹), lysozyme (200 µg ml⁻¹), 0.5% Triton X-100, 5 mM MgCl₂, and 1× protease inhibitor (MedChemExpress)] for 30 min at 37°C. After centrifugation of cell lysates (14,000 rpm, 10 min), the supernatant was ultracentrifuged at 150,000g for 60 min at 4°C. The pellet was suspended in 1 ml of sterile phosphate-buffered saline (PBS) after centrifugation. After another centrifugation at 14,000 rpm for 10 min at 4°C, the supernatant was ultracentrifuged for the second time at 150,000g for 60 min at 4°C to pellet the protein complex. The pellet was resuspended in 200 µl of ice-cold PBS and centrifuged at 14,000 rpm for 10 min at 4°C. The supernatant containing the PVC complex was stored at 4°C for short-term usage.

In vivo degradation PVC effectors

Stability of PVC effectors with or without their SP in *E. coli* was observed using *in vivo* degradation assays. Overnight culture of bacterial cells harboring the corresponding plasmids were inoculated (1:50) and grown at 37°C for approximately 2 hours. The chloramphenicol was then added to block the protein translation. Samples were taken at different time points, and PVC effectors were detected by Western blotting.

Immunoprecipitation assays and MS analysis

For immunoprecipitation assays, bacterial pellets producing PVC and its cognate effectors from exponential phase culture were lysed in buffer P, and the supernatants were collected after centrifuge. Anti-FLAG M2 magnetic beads (Sigma-Aldrich) were added in the supernatant and incubated with rotation for 1 hour at room temperature. The beads were washed three times with ice-cold PBS, and the bound proteins were eluted by competitive elution with the FLAG peptide solution. The samples were loaded on the protein gel for SDS-polyacrylamide gel electrophoresis (SDS-PAGE), and the

protein bands of interest were excised from the gels. The gels were treated routinely and then digested with trypsin and chymotrypsin enzyme solution. The digested peptides were extracted from the gels and lyophilized. Resuspended peptides in 0.1% formic acid were applied for liquid chromatography–tandem MS analysis (BiotechPack Scientific, Beijing). Raw MS files were searched against the *P. asymbotica* ATCC43949 protein database (UniProt). The N terminus of the protein of interest was determined from the results of two enzyme digestions.

Western blot analysis

The purified empty or filled PVC particles were heated at 100°C for 10 min with 1× SDS loading buffer. The samples were then loaded on the Novex 4 to 20% tris-glycine protein gel for separation. The gels were transferred to nitrocellulose membrane (Millipore) using a Bio-Rad semidry blotter. Standard protocols for membrane probing were conducted to detect the protein bands of interest. The detections were performed by using goat anti-rabbit/mouse secondary antibody (horseradish peroxidase) and Pierce ECL Plus Western blotting substrate and then visualized by Tanon 5200 (Tanon). The following primary antibodies were used: anti-Flag (clone M2) monoclonal antibody (Sigma-Aldrich, F3165), anti-RNA polymerase β monoclonal antibody (Abcam, ab191598), anti-mRFP (Origene, TA180093), anti-p65 (C terminus, Santa Cruz Biotechnology, sc-372), anti-p65 (N terminus, Santa Cruz Biotechnology, sc-8008), anti- β -actin (Abcam, ab6276), anti-Akt (Cell signaling technology, 4685), and anti-Phospho-Akt Ser⁴⁷³ (Cell Signaling Technology, 4060). Anti-Pvc16, anti-Pnf, and anti-Pdp1 were generated from immunized rabbit serum using specific synthesized oligopeptides (Genscript).

PVC treatment of J774 cells and protein translocation assays

J774 cells (100 μ l) were grown to 70% confluency in 96-well plates as described. The concentration of purified PVC solution was determined using Nanodrop Spectrophotometer (Thermo Fisher Scientific). In general, for translocation of diverse cargo proteins by PVC into macrophages, PVC solution (250 μ g ml⁻¹; unless indicated) was added in each well, and incubation was performed for 24 or 48 hours at 37°C before detection or imaging. Experiments were performed at least three times, and the representative pictures were shown. Cell viability was determined by using the Cell Counting Kit-8 (MedChemExpress). Cells were lysed using cell lysis buffer for Western blot and immunoprecipitation (Beyotime Biotechnology), and Western blot was carried out with primary antibodies as indicated in the text.

For translocation of BlaM reporter protein, PVC-treated cells were washed with PBS and added with CCF2-AM (Invitrogen) for 60 min at room temperature. Fluorescence was monitored using a microplate reader at an excitation of 410 nm. Translocation was determined as a ratio of cleaved (460 nm, blue) to uncleaved (530 nm, green) signal. Samples were also observed with a Nikon fluorescence microscope. For translocation of Rluc protein, similar operations were conducted, and the luciferase were detected by using the *Renilla*-Glo Luciferase Assay System (Promega).

Electron microscopy

Negative staining was used to assess the sample homogeneity and concentration. Aliquots of 4 μ l of PVC samples were applied to glow-discharged copper grids, washed, and stained with 2% uranyl acetate. The negative-stained grids were examined on an FEI Tecnai T20 electron microscope operated at 120 kV.

For cryo-grid preparation, aliquots of 4 μ l of samples were applied to glow-discharged holey-carbon copper grids (Quantifoil, Germany, R1.2/1.3, 400 mesh) inside the chamber of an FEI Vitroto IV (4°C and 100% humidity). The cryo-grids were screened using an FEI Talos Arctica microscope operated at 200 kV. Data acquisition was performed using an FEI Titan Krios operated at 300 kV. Images were recorded using a GIF K2 camera (Gatan, USA) with SerialEM (50) in the superresolution counting and movie mode, at a nominal magnification of $\times 105,000$, corresponding to a calibrated pixel size of 0.678 Å at object scale (superresolution), with defocus ranging from 0.7 to 2.5 μ m. A total of 32 frames were collected for each movie stack. The dose rate was 4.9 e⁻ Å⁻² s⁻¹ with a total exposure time of 6.4 s.

Image processing

For PVC-PIdA sample, 3011 movie stacks were collected (fig. S4A). Drift correction and electron dose weighting were applied to movie stacks using MotionCor2 (51), generating summed images with or without dose weighting. The parameters of contrast transfer function were evaluated by CTFFIND4 (52) based on images without dose weighting. Micrographs were manually screened using RELION3.0 (53). A total of 56,993 particles, corresponding to the baseplate region, were then autopicked by Topaz (54). After rounds of two-dimensional (2D) classification (fig. S4B), 11,856 baseplate particles were selected for 3D refinement with C6 symmetry imposed, rendering a density map at 5.4-Å resolution (fig. S4C). For the region of sheath-tube trunk, particle centers were moved to the following sheath-tube trunk part based on the coordinates of baseplate particles, and a new set of particles were reextracted. A total of 8765 reextracted particles were subjected to 3D refinement with C6 symmetry, leading to a final density map at 10.8 Å (fig. S4D). All the resolution estimation was based on gold-standard Fourier shell correlation at the cutoff of 0.143. The maps were sharpened by auto-evaluated B-factors using RELION3.0 and examined using UCSF Chimera (55).

mRFP unfolding assays

JM109 (DE3) cells coproducing Pvc15 and various mRFP variants were cultured overnight and inoculated 1:100 into a 24-well plate for growth at 30°C. Isopropyl- β -D-thiogalactopyranoside (0.2 mM) was added into each well after 60 min, and the cultures were incubated for 20 hours with shaking. The optical density and mRFP fluorescence were monitored at 2-hour intervals in a SYNERGY Neo plate reader (BioTek). The relative changes of mRFP fluorescence intensity in the cultures were determined.

PVC treatment of tumor cells in mouse model

This study with mice was conducted by Biocytogen in accordance with Association for Assessment and Accreditation of Laboratory Animal Care guidelines. This study was approved by Biocytogen's Institutional Animal Care and Use Committee and in compliance with the Guide for the Care and Use of Laboratory Animals (National Research Council, 2011). The experiments were performed on female BALB/c mice aged 6 to 8 weeks. The J774A.1 cells were subcutaneously implanted on the right (1×10^7 cells per mouse). The mice were divided into three groups randomly (five per group). When the tumor volume reached approximately 80 mm³, the mice were injected with the PBS or PVC solutions intratumorally at a dose of 30 mg/kg, three times per week, in a period of 18 days.

The tumor volume and body weight were measured twice per week. At the end point, the mice were euthanized, and the tumors were harvested for examination.

Bioinformatics and statistical analysis

All sequences were obtained from National Center for Biotechnology Information/Uniprot. Multiple sequence alignments and phylogenetic analysis were performed using Clustal Omega and MEGA7 (56, 57). Sequence logo was created using Weblogo application (58). Two-sample *t* test comparisons were performed to confirm statistical significance at 95% confidence between the samples compared (***P* < 0.001, ***P* < 0.01, and **P* < 0.05).

SUPPLEMENTARY MATERIALS

Supplementary material for this article is available at <https://science.org/doi/10.1126/sciadv.abm2343>

[View/request a protocol for this paper from Bio-protocol.](#)

REFERENCES AND NOTES

1. S. Wettstadt, A. Filloux, Manipulating the type VI secretion system spike to shuttle passenger proteins. *PLoS ONE* **15**, e0228941 (2020).
2. E. Del Tordello, O. Danilchanka, A. J. McCluskey, J. J. Mekalanos, Type VI secretion system sheaths as nanoparticles for antigen display. *PNAS* **113**, 3042–3047 (2016).
3. F. Bai, Z. P. Li, A. Umezawa, N. Terada, S. G. Jin, Bacterial type III secretion system as a protein delivery tool for a broad range of biomedical applications. *Biotechnol. Adv.* **36**, 482–493 (2018).
4. J. E. Galan, M. Lara-Tejero, T. C. Marlovits, S. Wagner, Bacterial type III secretion systems: Specialized nanomachines for protein delivery into target cells. *Annu. Rev. Microbiol.* **68**, 415–438 (2014).
5. H. A. Pendergrass, A. E. May, Delivery of heterologous proteins, enzymes, and antigens via the bacterial type III secretion system. *Microorganisms* **8**, 777 (2020).
6. D. Park, M. Lara-Tejero, M. N. Waxham, W. W. Li, B. Hu, J. E. Galan, J. Liu, Visualization of the type III secretion mediated Salmonella-host cell interface using cryo-electron tomography. *eLife* **7**, e39514 (2018).
7. D. Meusch, C. Gatsogiannis, R. G. Efremov, A. E. Lang, O. Hofnagel, I. R. Vetter, K. Aktories, S. Raunser, Mechanism of Tc toxin action revealed in molecular detail. *Nature* **508**, 61–65 (2014).
8. C. Gatsogiannis, F. Merino, D. Roderer, D. Balchin, E. Schubert, A. Kuhlee, M. Hayer-Hartl, S. Raunser, Tc toxin activation requires unfolding and refolding of a beta-propeller. *Nature* **563**, 209–213 (2018).
9. D. Roderer, O. Hofnagel, R. Benz, S. Raunser, Structure of a Tc holotoxin pore provides insights into the translocation mechanism. *Proc. Natl. Acad. Sci. U.S.A.* **116**, 23083–23090 (2019).
10. D. Roderer, E. Schubert, O. Sitsel, S. Raunser, Towards the application of Tc toxins as a universal protein translocation system. *Nat. Commun.* **10**, 5263 (2019).
11. P. N. Ng'ang'a, J. K. Ebner, M. Plessner, K. Aktories, G. Schmidt, Engineering photorhabdus luminescens toxin complex (PTC) into a recombinant injection nanomachine. *Life Sci Alliance* **2**, e201900485 (2019).
12. F. Jiang, N. Li, X. Wang, J. Cheng, Y. Huang, Y. Yang, J. Yang, B. Cai, Y. P. Wang, Q. Jin, N. Gao, Cryo-EM structure and assembly of an extracellular contractile injection system. *Cell* **177**, 370–383.e15 (2019).
13. X. Wang, J. Cheng, J. Shen, L. Liu, N. Li, N. Gao, F. Jiang, Q. Jin, Characterization of photorhabdus virulence cassette as a causative agent in the emerging pathogen photorhabdus asymbiotica. *Sci. China Life Sci.* (2022).
14. X. Wang, J. Shen, F. Jiang, Q. Jin, The photorhabdus virulence cassettes RRSP-like effector interacts with cyclin-dependent kinase 1 and causes mitotic defects in mammalian cells. *Front. Microbiol.* **11**, 366 (2020).
15. G. Yang, A. J. Dowling, U. Gericke, R. H. French-Constant, N. R. Waterfield, Photorhabdus virulence cassettes confer injectable insecticidal activity against the wax moth. *J. Bacteriol.* **188**, 2254–2261 (2006).
16. P. Wilkinson, N. R. Waterfield, L. Crossman, C. Corton, M. Sanchez-Contreras, I. Vlisidou, A. Barron, A. Bignell, L. Clark, D. Ormond, M. Mayho, N. Bason, F. Smith, M. Simmonds, C. Churcher, D. Harris, N. R. Thompson, M. Quail, J. Parkhill, R. H. French-Constant, Comparative genomics of the emerging human pathogen Photorhabdus asymbiotica with the insect pathogen Photorhabdus luminescens. *BMC Genomics* **10**, 302 (2009).
17. V. Deruelle, S. Bouillot, V. Job, E. Taillebourg, M. O. Fauvarque, I. Attree, P. Huber, The bacterial toxin ExoU requires a host trafficking chaperone for transportation and to induce necrosis. *Nat. Commun.* **12**, 4024 (2021).
18. H. A. Howell, L. K. Logan, A. R. Hauser, Type III secretion of ExoU is critical during early pseudomonas aeruginosa pneumonia. *MBio* **4**, e00032-13 (2013).
19. A. Hodgson, E. M. Wier, K. Fu, X. Sun, H. B. Yu, W. X. Zheng, H. P. Sham, K. Johnson, S. Bailey, B. A. Vallance, F. Y. Wan, Metalloprotease NleC suppresses host NF-κB/inflammatory responses by cleaving p65 and interfering with the p65/RPS3 interaction. *PLoS Pathog.* **11**, e1004705 (2015).
20. M. Suzuki, H. Mimuro, K. Kiga, M. Fukumatsu, N. Ishijima, H. Morikawa, S. Nagai, S. Koyasu, R. H. Gilman, D. Kersulyte, D. E. Berg, C. Sasakawa, Helicobacter pylori CagA phosphorylation-independent function in epithelial proliferation and inflammation. *Cell Host Microbe* **5**, 23–34 (2009).
21. A. G. Kinshikar, I. Verma, D. Chandra, K. K. Singh, K. Welding, P. Andersen, T. D. Hsu, W. R. Jacobs, S. Laal, Potential role for ESAT6 in dissemination of M. tuberculosis via human lung epithelial cells. *Mol. Microbiol.* **75**, 92–106 (2010).
22. F. Jiang, N. R. Waterfield, J. Yang, G. Yang, Q. Jin, A pseudomonas aeruginosa type VI secretion phospholipase D effector targets both prokaryotic and eukaryotic cells. *Cell Host Microbe* **15**, 600–610 (2014).
23. A. B. Russell, M. LeRoux, K. Hathazi, D. M. Agnello, T. Ishikawa, P. A. Wiggins, S. N. Wai, J. D. Mougous, Diverse type VI secretion phospholipases are functionally plastic antibacterial effectors. *Nature* **496**, 508–512 (2013).
24. T. Tobe, S. A. Beaton, H. Taniguchi, H. Abe, C. M. Bailey, A. Fivian, R. Younis, S. Matthews, O. Marches, G. Frankel, T. Hayashi, M. J. Pallen, An extensive repertoire of type III secretion effectors in Escherichia coli O157 and the role of lambdaoid phages in their dissemination. *PNAS* **103**, 14941–14946 (2006).
25. D. D. Majewski, L. J. Worrall, C. Hong, C. E. Atkinson, M. Vuckovic, N. Watanabe, Z. H. Yu, N. C. J. Strynadka, Cryo-EM structure of the homohexameric T355 ATPase-central stalk complex reveals rotary ATPase-like asymmetry. *Nat. Commun.* **10**, 626 (2019).
26. D. Chetrit, B. Hu, P. J. Christie, C. R. Roy, J. Liu, A unique cytoplasmic ATPase complex defines the Legionella pneumophila type IV secretion channel. *Nat. Microbiol.* **3**, 678–686 (2018).
27. N. Kapitein, G. Bonemann, A. Pietrosiuk, F. Seyffer, I. Hausser, J. K. Locker, A. Mogk, ClpV recycles VipA/VipB tubules and prevents non-productive tubule formation to ensure efficient type VI protein secretion. *Mol. Microbiol.* **87**, 1013–1028 (2013).
28. Y. Tang, J. Liang, A. Wu, Y. Chen, P. Zhao, T. Lin, M. Zhang, Q. Xu, J. Wang, Y. Huang, Co-delivery of trichosanthin and albendazole by nano-self-assembly for overcoming tumor multidrug-resistance and metastasis. *ACS Appl. Mater. Interfaces* **9**, 26648–26664 (2017).
29. W. W. Shi, K. B. Wong, P. C. Shaw, Structural and functional investigation and pharmacological mechanism of trichosanthin, a type 1 ribosome-inactivating protein. *Toxins (Basel)* **10**, 335 (2018).
30. B. Jana, K. Keppel, D. Salomon, Engineering a customizable antibacterial T6SS-based platform in vibrio natriegens. *EMBO Rep.* **22**, e53681 (2021).
31. S. J. Hersch, L. Lam, T. G. Dong, Engineered type six secretion systems deliver active exogenous effectors and cre recombinase. *MBio* **12**, e0111521 (2021).
32. J. L. Berry, V. Pelicic, Exceptionally widespread nanomachines composed of type IV pilins: The prokaryotic swiss army knives. *FEMS Microbiol. Rev.* **39**, 134–154 (2015).
33. J. P. Barnier, D. Euphrasie, O. Join-Lambert, M. Audry, S. Schonherr-Hellec, T. Schmitt, S. Bourdoulous, M. Coureuil, X. Nassif, M. El Behi, Type IV pilus retraction enables sustained bacteremia and plays a key role in the outcome of meningococcal sepsis in a humanized mouse model. *PLoS Pathog.* **17**, e1009299 (2021).
34. A. T. S. Jean, C. A. Swofford, J. T. Panteli, Z. J. Brentzel, N. S. Forbes, Bacterial delivery of staphylococcus aureus α-hemolysin causes regression and necrosis in murine tumors. *Mol. Ther.* **22**, 1266–1274 (2014).
35. S. Koo, S. Cheley, H. Bayley, Redirecting pore assembly of staphylococcal α-hemolysin by protein engineering. *ACS Cent Sci* **5**, 629–639 (2019).
36. S. B. Zhou, C. Gravekamp, D. Bermudes, K. Liu, Tumor-targeting bacteria engineered to fight cancer. *Nat. Rev. Cancer* **18**, 727–743 (2018).
37. S. Wagner, I. Grin, S. Malmshemer, N. Singh, C. E. Torres-Vargas, S. Westerhausen, Bacterial type III secretion systems: A complex device for the delivery of bacterial effector proteins into eukaryotic host cells. *FEMS Microbiol. Lett.* **365**, fny201 (2018).
38. K. Manera, F. Kamal, B. Burkinshaw, T. G. Dong, Essential functions of chaperones and adaptors of protein secretion systems in gram-negative bacteria. *FEBS J.* **1–14** (2021).
39. A. G. Portaliou, K. C. Tsolis, M. S. Loos, V. Zorzini, A. Economou, Type III secretion: Building and operating a remarkable nanomachine. *Trends Biochem. Sci.* **41**, 175–189 (2016).
40. D. Frenkiel-Krispin, S. G. Wolf, S. Albeck, T. Unger, Y. Peleg, J. Jacobovitch, Y. Michael, S. Daube, M. Sharon, C. V. Robinson, D. I. Svergun, D. F. Fass, T. Tzfira, M. Elbaum, Plant transformation by agrobacterium tumefaciens: Modulation of single-stranded DNA-VirE2 complex assembly by VirE. *J. Biol. Chem.* **282**, 3458–3464 (2007).
41. J. P. Xu, D. D. Xu, M. Y. Wan, L. Yin, X. F. Wang, L. J. Wu, Y. H. Liu, X. Y. Liu, Y. Zhou, Y. Q. Zhu, Structural insights into the roles of the IcmS-IcmW complex in the type IVb secretion system of Legionella pneumophila. *PNAS* **114**, 13543–13548 (2017).

42. A. Tohidpour, CagA-mediated pathogenesis of *Helicobacter pylori*. *Microb Pathogenesis* **93**, 44–55 (2016).
43. A. M. Geller, I. Pollin, D. Zlotkin, A. Danov, N. Nachmias, W. B. Andreopoulos, K. Shemesh, A. Levy, The extracellular contractile injection system is enriched in environmental microbes and associates with numerous toxins. *Nat. Commun.* **12**, 3743 (2021).
44. B. J. Burkinshaw, X. Liang, M. Wong, A. N. H. Le, L. Lam, T. G. Dong, A type VI secretion system effector delivery mechanism dependent on PAAR and a chaperone-co-chaperone complex. *Nat. Microbiol.* **3**, 632–640 (2018).
45. S. Ahmad, K. K. Tsang, K. Sachar, D. Quentin, T. M. Tashin, N. P. Bullen, S. Raunser, A. G. McArthur, G. Prehna, J. C. Whitney, Structural basis for effector transmembrane domain recognition by type VI secretion system chaperones. *eLife* **9**, e62816 (2020).
46. J. C. Whitney, D. Quentin, S. Sawai, M. LeRoux, B. N. Harding, H. E. Ledvina, B. Q. Tran, H. Robinson, Y. A. Goo, D. R. Goodlett, S. Raunser, J. D. Mougous, An interbacterial NAD(P) (+) glycohydrolase toxin requires elongation factor Tu for delivery to target cells. *Cell* **163**, 607–619 (2015).
47. B. Berni, C. Soscia, S. Djermoun, B. Ize, S. Bleves, A type VI secretion system trans-kingdom effector is required for the delivery of a novel antibacterial toxin in *Pseudomonas aeruginosa*. *Front. Microbiol.* **10**, 1218 (2019).
48. D. D. Bondage, J. S. Lin, L. S. Ma, C. H. Kuo, E. M. Lai, VgrG C terminus confers the type VI effector transport specificity and is required for binding with PAAR and adaptor-effector complex. *P Natl Acad Sci USA* **113**, E3931–E3940 (2016).
49. W. Jiang, X. Zhao, T. Gabrieli, C. Lou, Y. Ebenstein, T. F. Zhu, Cas9-assisted targeting of Chromosome segments CATCH enables one-step targeted cloning of large gene clusters. *Nat. Commun.* **6**, 8101 (2015).
50. D. N. Mastronarde, Automated electron microscope tomography using robust prediction of specimen movements. *J. Struct. Biol.* **152**, 36–51 (2005).
51. S. Q. Zheng, E. Palovcak, J. P. Armache, K. A. Verba, Y. Cheng, D. A. Agard, MotionCor2: Anisotropic correction of beam-induced motion for improved cryo-electron microscopy. *Nat. Methods* **14**, 331–332 (2017).
52. A. Rohou, N. Grigorieff, CTFFIND4: Fast and accurate defocus estimation from electron micrographs. *J. Struct. Biol.* **192**, 216–221 (2015).
53. J. Zivanov, T. Nakane, B. O. Forsberg, D. Kimanius, W. J. H. Hagen, E. Lindahl, S. H. W. Scheres, New tools for automated high-resolution cryo-EM structure determination in RELION-3. *eLife* **7**, e42166 (2018).
54. T. Bepler, A. Morin, M. Rapp, J. Brasch, L. Shapiro, A. J. Noble, B. Berger, Positive-unlabeled convolutional neural networks for particle picking in cryo-electron micrographs. *Nat. Methods* **16**, 1153–1160 (2019).
55. E. F. Pettersen, T. D. Goddard, C. C. Huang, G. S. Couch, D. M. Greenblatt, E. C. Meng, T. E. Ferrin, UCSF Chimera—A visualization system for exploratory research and analysis. *J. Comput. Chem.* **25**, 1605–1612 (2004).
56. F. Sievers, A. Wilm, D. Dineen, T. J. Gibson, K. Karplus, W. Li, R. Lopez, H. McWilliam, M. Remmert, J. Soding, J. D. Thompson, D. G. Higgins, Fast, scalable generation of high-quality protein multiple sequence alignments using Clustal Omega. *Mol. Syst. Biol.* **7**, 539 (2011).
57. S. Kumar, G. Stecher, K. Tamura, MEGA7: Molecular evolutionary genetics analysis version 7.0 for bigger datasets. *Mol. Biol. Evol.* **33**, 1870–1874 (2016).
58. G. E. Crooks, G. Hon, J. M. Chandonia, S. E. Brenner, WebLogo: A sequence logo generator. *Genome Res.* **14**, 1188–1190 (2004).

Acknowledgments: We thank the cryo-EM platform of Peking University and the Electron Microscopy Laboratory of Peking University for the data collection. We also thank the Core Facilities at the School of Life Sciences, Peking University for help with negative-staining EM and the National Center for Protein Sciences at Peking University for assistance in sample preparation. The computation was supported by High-performance Computing Platform of Peking University. **Funding:** The project was funded by the CAMS Innovation Fund for Medical Sciences (2021-I2M-1-037 to F.J.) and the National Natural Science Foundation of China (NSFC) (32070081 and 31870108 to F.J. and 32000080 to X.W.); the Beijing Natural Science Foundation (5192019 to F.J.); and the Fundamental Research Funds for the Central Universities (3332021092 to F.J.). The work was also supported by the National Key Research and Development Program of China (2019YFA0508904 to N.G.) and the National Science Foundation of China (31725007 and 31630087 to N.G. and 31922036 to N.L.). **Author contributions:** F.J., J.S., J.C., X.W., J.Y., and N.L. performed the experiments and analyzed the data. N.G. and Q.J. provided advice on the project. F.J., N.G., and Q.J. conceived the project, designed experiments, and wrote the manuscript. **Competing interests:** The authors declare that they have no competing interests. **Data and materials availability:** All data needed to evaluate the conclusions in the paper are present in the paper and/or the Supplementary Materials. Cryo-EM maps have deposited in the EMDB: PVC-PldA baseplate (EMDB-31709) and PVC-PldA trunk (EMDB-31710).

Submitted 3 September 2021

Accepted 11 February 2022

Published 29 April 2022

10.1126/sciadv.abm2343